Hindawi
Advances in Materials Science and Engineering
Volume 2017, Article ID 1759469, 7 pages
https://doi.org/10.1155/2017/1759469

Research Article

Fabrication of Metal Nanoparticle Arrays in the $ZrO_2(Y)$, $HfO_2(Y)$, and GeO_x Films by Magnetron Sputtering

Oleg Gorshkov,[1] Ivan Antonov,[2] Dmitry Filatov,[1] Maria Shenina,[1] Alexander Kasatkin,[2] Alexander Bobrov,[1] Maria Koryazhkina,[2] Irina Korotaeva,[3] and Mikhail Kudryashov[3]

[1]*Research and Educational Center for Physics of Solid State Nanostructures, Lobachevsky State University of Nizhny Novgorod, 23 Gagarin Ave., Nizhny Novgorod 603950, Russia*
[2]*Research Institute for Physics and Technology, Lobachevsky State University of Nizhny Novgorod, 23 Gagarin Ave., Nizhny Novgorod 603950, Russia*
[3]*Department of Physics, Lobachevsky State University of Nizhny Novgorod, 23 Gagarin Ave., Nizhny Novgorod 603950, Russia*

Correspondence should be addressed to Dmitry Filatov; dmitry_filatov@inbox.ru

Received 20 April 2017; Accepted 11 June 2017; Published 12 July 2017

Academic Editor: Ilia Ivanov

The single sheet arrays of Au nanoparticles (NPs) embedded into the $ZrO_2(Y)$, $HfO_2(Y)$, and GeO_x ($x \approx 2$) films have been fabricated by the alternating deposition of the nanometer-thick dielectric and metal films using Magnetron Sputtering followed by annealing. The structure and optical properties of the NP arrays have been studied, subject to the fabrication technology parameters. The possibility of fabricating dense single sheet Au NP arrays in the matrices listed above with controlled NP sizes (within 1 to 3 nm) and surface density has been demonstrated. A red shift of the plasmonic optical absorption peak in the optical transmission spectra of the nanocomposite films (in the wavelength band of 500 to 650 nm) has been observed. The effect was attributed to the excitation of the collective surface plasmon-polaritons in the dense Au NP arrays. The nanocomposite films fabricated in the present study can find various applications in nanoelectronics (e.g., single electronics, nonvolatile memory devices), integrated optics, and plasmonics.

1. Introduction

In recent years, the investigations of the optical and electronic properties of the metal nanoparticles (MNPs) embedded into various dielectric matrices have attracted much attention [1]. These nanocomposite materials are promising for the applications in nonvolatile memory [2–5], single electronics [6], integrated optics [7], plasmonics [8], and so forth. For instance, the MNPs are known to play a role of the electromagnetic field concentrators in the resistive random access memory (RRAM) cells and, therefore, to improve the stability of these ones [4] and to increase the yield of the RRAM devices [2]. In the last decade, a new direction in the studies of the dielectric films with embedded MNPs has emerged, namely, the investigations of the photoconductivity in the MNP arrays in the dielectric films due to the optically excited plasmon resonance (PR) in the MNP arrays. The motivation for this activity was to control the conductivity of the nanocomposite materials by means of the optical pumping in the visible wavelength band [9].

Ion implantation with subsequent annealing is used widely to fabricate the MNPs in the dielectric matrices [10]. This method allows forming the MNPs with controlled sizes and densities within a wide range. However, the MNPs formed by ion implantation are featured by an essential scatter in sizes originating from the stochastic nature of the ion interaction with solids. The alternating deposition of the metal and dielectric films (e.g., by Electron Beam Evaporation or by Magnetron Sputtering) with subsequent annealing is another method applied to fabricate the MNP arrays in the dielectric matrices [11]. The metal film material coagulates into the MNPs during annealing thus forming the single

sheet MNP arrays separated by the dielectric spacers with the predefined thickness. The Au nanoparticle (NP) arrays in the SiO_2 matrix have been studied most comprehensively to date, mainly, due to poor solubility and diffusivity of Au in SiO_2 [12] that favors the coagulation of the Au films into the NPs. On the other hand, yttria-stabilized zirconia ZrO_2(Y) and hafnia HfO_2(Y) [4, 13] as well as germanium dioxide GeO_2 [14] are promising oxide matrices for various applications. However, the structure and the optical properties of the MNP arrays in the nanocomposite films formed by Magnetron Sputtering from the above materials have been studied insufficiently to date.

In [14, 15], we have reported the fabrication of dense Au NP arrays inside the ZrO_2(Y) films using layer-by-layer Magnetron Sputtering followed by annealing. The uniform Au NPs of 1 to 3 nm in diameter (subject to the initial Au film thickness) were arranged in a single sheet inside the ZrO_2(Y) films. The optical transmission spectra measurements revealed a red shift of the plasmon absorption peaks in the Au NPs (down to ~650 nm) attributed to the collective plasmon excitation in the dense NP arrays.

It should be noted that dense enough Au NP arrays in the oxide matrices specified above manifesting the collective plasmonic excitations could be fabricated by ion implantation as well [16]. However, forming the high density NP arrays requires high enough ion doses that in turn leads to high concentration of the radiation defects. From this viewpoint, Magnetron Sputtering has a considerable advantage as compared to ion implantation in forming the dense NP arrays because Magnetron Sputtering provides the formation of more uniform NPs in the defect-free dielectric matrix.

In the present paper, the results of comprehensive studies of the structure and optical properties of the Au NP arrays in the ZrO_2(Y), HfO_2(Y), and GeO_x ($x \approx 2$) films formed with layer-by-layer Magnetron Sputtering subject to the conditions of the deposition process are reported. The purpose of the present study was to investigate the capabilities of Magnetron Sputtering in forming the MNP arrays in the above dielectric matrices with controlled morphology and optical properties necessary for various nanoelectronic and photonic applications.

2. Materials and Methods

The samples for investigations were fabricated by Magnetron Sputtering using Torr International 2g1-1g2-eb4-th1 vacuum setup for thin film deposition on the fused silica and Si(100) substrates. The underlying oxide layers 20 nm in thickness were deposited on the substrate surface by radio frequency (RF) Magnetron Sputtering in the Ar-O_2 gas mixture (50-50% mol.) at the substrate temperature $T_g = 300 \pm 10^{\circ}$C. Then, the islanded Au films with nominal thickness $d_{Au} = 0.5$, 1.0, and 2.0 nm were deposited by direct current (dc) Magnetron Sputtering in Ar ambient at $T_g = 200 \pm 10^{\circ}$C. Finally, the Au films were capped by the cladding layers of the same dielectric with the thickness of 20 nm. So far, the overall thickness of the nanocomposite films was ≈ 40 nm. The oxide/Au/oxide stacks were annealed in the Ar flow at the temperature $T_A = 450 \pm 10^{\circ}$C in order to make the islanded Au films coagulate into the NPs. The annealing times t_A were 2 min, 1 hr, and 2 hrs. Also, the 40 nm thick dielectric films without the NPs were fabricated to serve as the reference samples.

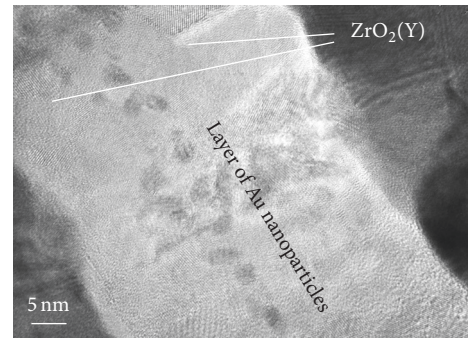

Figure 1: High resolution X-TEM image of a ZrO_2(Y)/Au(1 nm)/ZrO_2(Y)/Si stack after annealing at 450°C for 2 min.

The investigations of the structure of the nanocomposite films deposited onto the Si substrates were carried out by High Resolution Cross-Sectional Transmission Electron Microscopy (HR X-TEM) using Jeol® JEM 2100/F electron microscope. The single crystal Si(100) substrates served as a reference in the HR TEM measurements with atomic resolution. The optical properties of the nanocomposite films formed on the fused silica substrates were investigated by optical transmission spectroscopy at 300 K using Varian® Cary™ 6000i spectrophotometer. The refractive indices of the reference dielectric films were measured by spectrum-resolved ellipsometry using MicroPhotonic® PhE-102 instrument.

3. Results and Discussion

The results of the structural investigations of the nanocomposite films by HR X-TEM have demonstrated that during annealing the islanded Au films transform into the two-dimensional arrays of almost round NPs. For example, Figure 1 presents a HR X-TEM image of a ZrO_2(Y)/Au(1 nm)/ZrO_2(Y)/Si stack after annealing at 450°C for 2 min. The TEM image shows the Au NPs with the diameter $D = 2.3 \pm 0.4$ nm and with the average surface density $N_s \approx 7.3 \cdot 10^{12}$ cm^{-2} to be confined almost in a single sheet in the middle of the dielectric film within a thin layer of ~10 nm thickness. The location of the NP layer inside the dielectric film is determined by the thicknesses of the underlying layer and of the cladding one. In the case of the stack, the TEM image of which is shown in Figure 1, the underlying layer and the cladding one had the same thickness ≈ 20 nm. The HR X-TEM images have shown also the Au NPs to have a single crystal structure whereas ZrO_2(Y) layers had a nanocrystalline structure with the grain sizes of 5 to 15 nm.

Figures 2(a), 2(b), and 2(c) present typical optical transmission spectra of the ZrO_2(Y)/Au/ZrO_2(Y)/SiO_2, HfO_2(Y)/Au/HfO_2(Y)/SiO_2, and GeO_2/Au/GeO_2/SiO_2 stacks for d_{Au} = 0.5 nm, 1.0 nm, and 2.0 nm, respectively, after annealing for

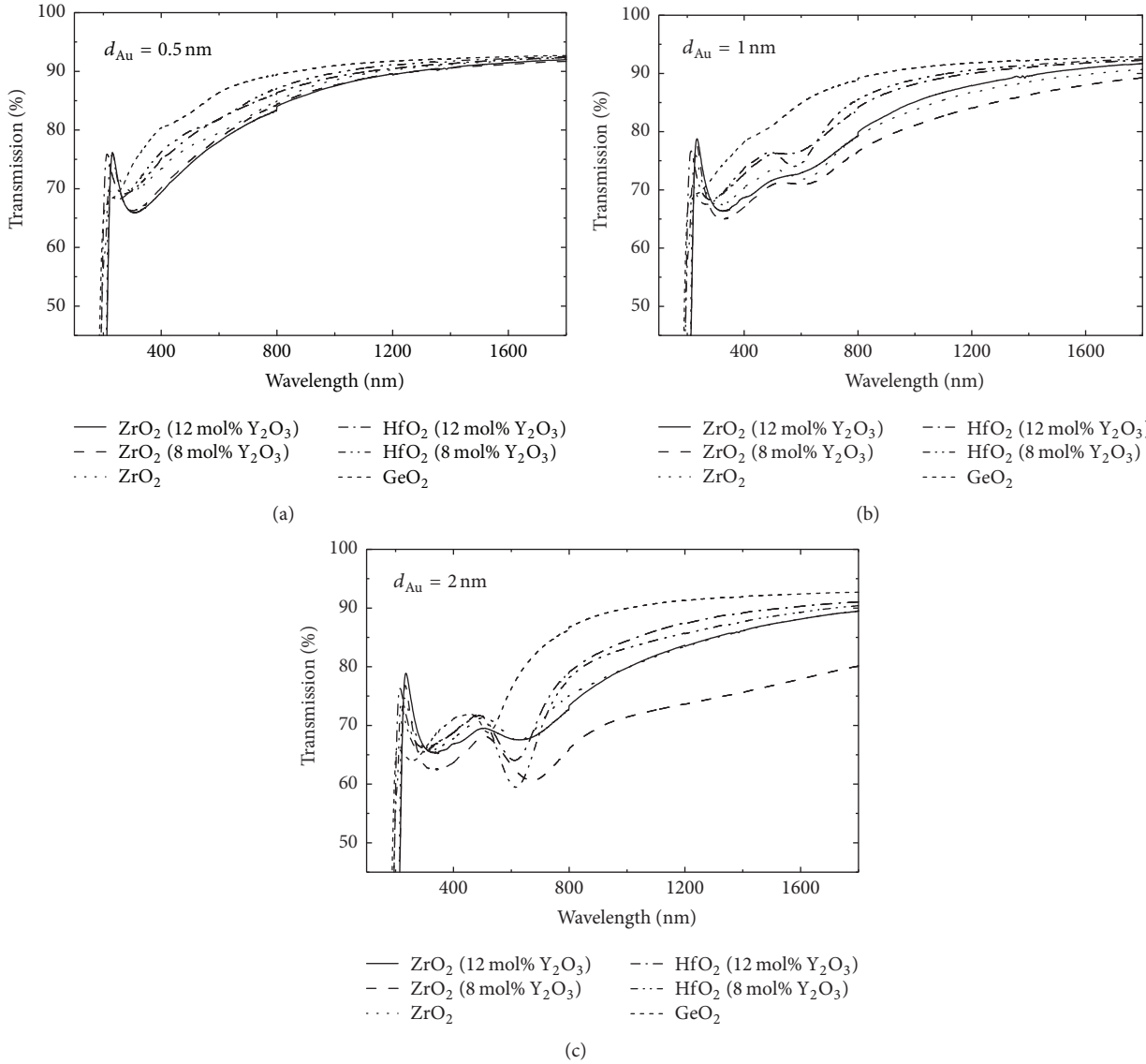

Figure 2: Typical optical transmission spectra (300 K) of $ZrO_2(Y)/Au/ZrO_2(Y)/SiO_2$, $HfO_2(Y)/Au/HfO_2(Y)/SiO_2$, and $GeO_2/Au/GeO_2/SiO_2$ stacks with different values of the nominal Au film thickness d_{Au} after annealing at 450°C for 1 hr.

1 hr. Besides a background due to the impurity absorption in the dielectric films and the interference fringes typical for the thin films, the plasmon absorption peaks in the Au NPs were observed in the optical transmission spectra.

In the $ZrO_2(Y)$- and $HfO_2(Y)$-based films, the PR peaks were observed at the wavelengths $\lambda \approx 623$ nm and ≈607 nm, respectively, while in the GeO_2-based film the PR peak was observed at $\lambda \approx 529$ nm. Different values of the spectral positions of the PR peaks observed for the Au NP arrays formed in the same conditions coincide with the differences in the refractive index n of the respective matrix materials (2.15 to 2.20 for $ZrO_2(Y)$, 1.95 to 2.05 for $HfO_2(Y)$, and ≈1.6 for GeO_2, according to the spectrum-resolved ellipsometry data for the probing light wavelength 632.8 nm), in full agreement with Mie scattering theory [17]. The scatter in the values of n obtained for the $ZrO_2(Y)$ and $HfO_2(Y)$ films was due to different molar fraction of Y_2O_3 in different samples [18]. It should be noted that a nonuniform distribution of Y in the host oxide films could introduce an additional scatter in the values of n measured in these ones as well [18].

It is worth noting that the expected PR peak wavelengths calculated for the separate Au NPs with the same sizes in the $ZrO_2(Y)$ and $HfO_2(Y)$ matrices according to Mie scattering theory [17] fall into the range from 590 to 600 nm. For the GeO_2 matrix, the expected PR peak wavelength was ≈470 nm. The red shift of the PR peak observed in the experiment relative to the calculated values for the noninteracting NPs was attributed to the collective plasmon excitation in dense Au NP arrays [19]. The parameter $a = D/l$, where l is the average spacing between the NPs, can serve as a criterion of the MNP array density [19]. For example, for the $ZrO_2(Y)/Au/ZrO_2(Y)/Si$ stack, the TEM image of which is shown in Figure 1, $a \sim 0.62$.

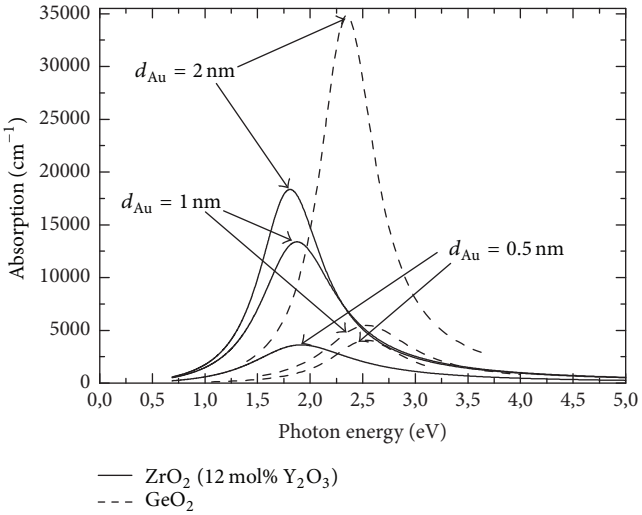

Figure 3: Plasmonic optical absorption spectra (300 K) of the ZrO_2(Y)/Au/ZrO_2(Y)/SiO_2 and GeO_2/Au/GeO_2/SiO_2 stacks after annealing at 450°C for 1 hr. The optical absorption spectra were calculated from the respective optical transmission ones presented in Figures 2(a) and 2(c).

It is worth noting that usually the oxide films deposited by RF Magnetron Sputtering are featured by a considerable excess surface charge density, which also could potentially induce a shift in the frequency of the plasmon resonance in the MNPs due to the charging of these ones [20]. Indeed, the *C-V* measurements performed on the *n*-Si(001)/ZrO_2(Y)/Au metal-oxide-semiconductor (MOS) stacks with the 40 nm thick ZrO_2(Y) layers deposited by RF Magnetron Sputtering in the same conditions as the ones studied in the present paper have revealed a built-in negative charge with the effective surface density ~ 10^{12} cm^{-2} [21]. However, the excess charging of the NPs with electrons would result in a blue shift of the plasmon resonance in these ones [20] whereas red shift of the plasmon resonance with respect to the bulk has been observed in the present paper. In any case, the effect of the excess charge in the MNPs on the absorption signatures of these ones is quite small and limited in very small NPs [22]. Note that just such NPs were the objects of investigations in the present study. So far, one can conclude that the collectivization of the plasmon excitations in the dense NP arrays rather than the charging of the NPs was the primary factor governing the optical properties of the NPs studied in the present work.

From the plasmonic optical absorption spectra (see, e.g., Figure 3) obtained from the transmission ones by standard technique, the average diameter D, surface density of NPs N_s, the volume fraction of the NPs N_v calculated for the 10 nm thick layer, within which the NPs are confined, and the array density parameter a have been evaluated using Mie scattering theory [17]. The results of the optical transmission data analysis for the annealing time t_A = 2 min, 1 hr, and 2 hrs are presented in Table 1. As shown in Table 1, the averaged NP diameter D and the array density parameter a as well as the relative volume fraction of NPs N_v increased with increasing nominal thickness of the initial Au film d_{Au} for all dielectric film materials. The values of a for the NPs arrays obtained from the TEM data and from the optical absorption spectra demonstrate the applicability of Magnetron Sputtering to fabricate the dense Au NP arrays in the ZrO_2(Y), HfO_2(Y), and GeO_2 thin films, in which the conditions for the manifestation of the collective plasmon excitations are provided.

The maximum values of a have been observed in ZrO_2(Y) and HfO_2(Y) with the Y_2O_3 molar fraction ≈ 0.12 and d_{Au} ≈ 2 nm that could be attributed to increased diffusivity of Au in the Y-stabilized zirconia and hafnia due to large concentration of the oxygen vacancies in these materials (the latter is equal to 1/2 of the one of Y [18]). So far, the greater the concentration of the stabilizing oxide Y_2O_3 in the film material, the better the conditions for the diffusion of Au, which promote the growth of the Au NPs during annealing. This conclusion was supported also by the fact that in the samples based on ZrO_2(Y) with the Y_2O_3 molar fraction ≈ 0.12 the values of the array density parameter a (as well as the ones of the surface density of the NPs N_s) were the largest as compared to other matrices as well as to other values of the Y_2O_3 molar fraction in ZrO_2(Y) and HfO_2(Y) for every value of d_{Au}. The smallest value of a has been observed in the sample based on amorphous GeO_2 (see Table 1). In the HfO_2(Y)-based samples, the doping by the stabilizing oxide Y_2O_3 affected the Au NP array density parameter a weaker than in the ZrO_2(Y)-based ones.

On the other hand, the concentration of Y_2O_3 affected the size of the NPs D formed in HfO_2(Y) as well as in ZrO_2(Y). The increasing of the Y_2O_3 molar fraction resulted in the decreasing of the NP diameter D accompanied by the corresponding increasing of the NP surface density for each value of d_{Au}. The largest values of NP diameter D have been observed in the undoped ZrO_2 and HfO_2 matrices.

Earlier, the NP diameter D in the ZrO_2(Y)-based nanocomposite films was found to increase with increasing nominal Au film thickness d_{Au} for all values of the annealing time t_A within the range from 2 min to 2 hrs [15]. The results obtained within the present study have revealed, in general, the same behavior of D with increasing d_{Au} for the HfO_2(Y)-based films as well as for the GeO_2-bases ones. However, the smallest NPs with D ≈ 0.72 nm and N_s ≈ $3.4 \cdot 10^{13}$ cm^{-2} have been observed in ZrO_2 with the highest concentration of Y_2O_3 and d_{Au} = 0.5 nm and t_A = 2 hrs (see Table 1). In this case, the decrease of the NP diameter with increasing t_A was attributed to the dissolving of the Au NPs during annealing because the detachment of the Au atoms from the NPs begins to prevail over the attachment at long enough annealing time t_A [15].

The variation of the stabilizing oxide Y_2O_3 molar fraction in ZrO_2(Y) and HfO_2(Y) has been found to affect the density parameter a weakly (see Table 1). This observation can be explained as follows. As one can see from Table 1, in general, in the HfO_2(Y) based films as well as in the ZrO_2(Y)-based ones the NP diameter D increased with decreasing Y_2O_3 molar fraction at given d_{Au} and t_A. Again, this effect may be ascribed to the increase in the concentration of the vacancies in the oxygen sublattice with increasing Y concentration that,

Table 1: The average diameter D, the surface density N_s, the volume fraction N_v, and the array density parameter a for the Au NPs in the ZrO_2(Y), HfO_2(Y), and GeO_2 based nanocomposite films fabricated by Magnetron Sputtering followed by annealing. Uncertainty assessment for all parameters is ~15%.

d_{Au}, nm	t_A	Film material	D, nm	N_s, cm^{-2}	N_v	a
0.5	2 min	ZrO_2 (12 mol.% Y_2O_3) [15]	1.1	$4.7 \cdot 10^{12}$	0.0028	0.23
		ZrO_2 (8 mol.% Y_2O_3)	—	—	—	—
		HfO_2 (12 mol.% Y_2O_3)	—	—	—	—
		HfO_2 (0 mol.% Y_2O_3)	—	—	—	—
		GeO_2	—	—	—	—
0.5	1 hr	ZrO_2 (12 mol.% Y_2O_3) [15]	1.2	$1.1 \cdot 10^{13}$	0.0097	0.40
		ZrO_2 (8 mol.% Y_2O_3)	—	—	—	—
		ZrO_2	1.9	$2.8 \cdot 10^{12}$	0.0106	0.27
		HfO_2 (12 mol.% Y_2O_3)	—	—	—	—
		HfO_2 (0 mol.% Y_2O_3)	1.9	$3.0 \cdot 10^{12}$	0.0108	0.28
		GeO_2	1.8	$2.3 \cdot 10^{12}$	0.0065	0.23
0.5	2 hrs	ZrO_2 (12 mol.% Y_2O_3) [15]	0.72	$3.4 \cdot 10^{13}$	0.0068	0.42
1.0	2 min	ZrO_2 (12 mol.% Y_2O_3) [15]	1.9	$4.0 \cdot 10^{12}$	0.0151	0.38
		ZrO_2 (8 mol.% Y_2O_3)	2.7	$1.2 \cdot 10^{12}$	0.0115	0.29
		HfO_2 (12 mol.% Y_2O_3)	—	—	—	—
		HfO_2 (0 mol.% Y_2O_3)	2.1	$2.9 \cdot 10^{12}$	0.0147	0.30
		GeO_2	—	—	—	—
1.0	1 hr	ZrO_2 (12 mol.% Y_2O_3) [15]	1.6	$5.0 \cdot 10^{12}$	0.0281	0.36
		ZrO_2 (8 mol.% Y_2O_3)	2.6	$1.6 \cdot 10^{12}$	0.0147	0.31
		ZrO_2	3.0	$1.4 \cdot 10^{12}$	0.0180	0.34
		HfO_2 (12 mol.% Y_2O_3)	2.2	$2.5 \cdot 10^{12}$	0.0205	0.30
		HfO_2 (0 mol.% Y_2O_3)	3.6	$6.8 \cdot 10^{11}$	0.0164	0.32
		GeO_2	1.5	$6.0 \cdot 10^{12}$	0.0103	0.27
1.0	2 hrs	ZrO_2 (12 mol.% Y_2O_3) [15]	1.7	$8.6 \cdot 10^{12}$	0.0223	0.50
2.0	2 min	ZrO_2 (12 mol.% Y_2O_3) [15]	1.9	$8.3 \cdot 10^{12}$	0.0274	0.54
		ZrO_2 (8 mol.% Y_2O_3)	2.4	$6.3 \cdot 10^{12}$	0.0482	0.44
		HfO_2 (12 mol.% Y_2O_3)	2.2	$7.6 \cdot 10^{12}$	0.0421	0.43
		HfO_2 (0 mol.% Y_2O_3)	3.5	$1.9 \cdot 10^{12}$	0.0404	0.43
		GeO_2	2.0	$9.1 \cdot 10^{12}$	0.0410	0.42
2.0	1 hr	ZrO_2 (12 mol.% Y_2O_3) [15]	1.8	$1.1 \cdot 10^{13}$	0.0346	0.60
		ZrO_2 (8 mol.% Y_2O_3)	2.6	$3.7 \cdot 10^{12}$	0.0370	0.40
		ZrO_2	3.4	$1.2 \cdot 10^{12}$	0.0230	0.36
		HfO_2 (12 mol.% Y_2O_3)	3.2	$2.8 \cdot 10^{12}$	0.0576	0.45
		HfO_2 (0 mol.% Y_2O_3)	3.4	$2.4 \cdot 10^{12}$	0.0528	0.45
		GeO_2	2.2	$4.4 \cdot 10^{12}$	0.0488	0.36
2.0	2 hrs	ZrO_2 (12 mol.% Y_2O_3) [15]	1.9	$7.9 \cdot 10^{12}$	0.0284	0.53

in turn, facilitates the diffusion of Au from the NPs into the rest of the volume of the ZrO_2(Y) and HfO_2(Y) films during annealing. On the other hand, the surface density of the NPs N_s decreased with decreasing Y_2O_3 content. For example, in the case of ZrO_2(Y) film with $d_{Au} \approx 0.5$ nm annealed during $t_A \approx 1$ hr, a notable increase of the NP size D by ≈58% (from 1.2 nm up to 1.9 nm) along with the reduction of the surface density of the NPs N_s by ≈75% (from $1.1 \cdot 10^{13}$ cm^{-2} down to $2.8 \cdot 10^{12}$ cm^{-2}) with decreasing the Y_2O_3 molar fraction from 12% down to 0% had been observed. For the HfO_2(Y) based film, this tendency was hard to trace in the case of thin initial Au film ($d_{Au} \approx 0.5$ nm) and short annealing time ($t_A \approx 2$ min) because the plasmonic absorption peaks were manifested poorly in the optical transmission spectra of this series of samples. However, in the cases of $d_{Au} \approx 1.0$ and 2.0 nm for $t_A \approx 2$ min and 1 hr, this tendency was expressed clearly. For instance, for $d_{Au} \approx 1.0$ nm and $t_A \approx 1$ hr the sizes of the Au NPs increased by 64% (from ≈2.2 nm up to ≈3.6 nm) whereas N_s reduced by ≈73% (from ≈$2.5 \cdot 10^{12}$ cm^{-2} down to ≈$6.8 \cdot 10^{11}$ cm^{-2}) with decreasing of the Y_2O_3 molar fraction from 12% down to 0%. Note that the differences in the relative increasing of the Au NP sizes D and the decreasing

of N_s make 10 to 15% for each value of d_{Au} and each t_A, that is, fall into the uncertainties of the determination of the above parameters from the optical transmission spectra. So far, the variations of the NP volume fraction N_v as well as of the array density parameter a fall into the uncertainty limits. This tendency can also point to the redistribution of the Au atoms among the NPs in the array during annealing: the Au atoms detach from the smaller NPs and attach the bigger ones. The greater the stabilizing oxide Y_2O_3 molar fraction is (i.e., the greater the oxygen vacancy concentration), the more the redistribution is pronounced. Therefore, the decrease of the Y_2O_3 molar fraction complicates the diffusion of the Au atoms during annealing thus preventing the redistribution of these ones among the NPs and increasing the NP surface density.

4. Conclusion

The structural parameters and optical properties of the single sheet Au nanoparticle arrays formed inside the $ZrO_2(Y)$, $HfO_2(Y)$, and GeO_x ($x \approx 2$) nanometer-thick films with layer-by-layer Magnetron Sputtering deposition with subsequent annealing have been studied, subject to the technological parameters of the film fabrication process. The possibility of the fabrication of the single sheet Au nanoparticle arrays in the $ZrO_2(Y)$, $HfO_2(Y)$, and GeO_2 thin films positioned at a predefined distance from the substrate and from the film surface has been demonstrated. The technological regimes for forming the dense uniform Au nanoparticle arrays, in which the conditions for the collective plasmon excitations take place, were found. The fabricated nanocomposite films can find various applications used in single electronic devices, nonvolatile memory, integrated optics, and plasmonics.

Conflicts of Interest

The authors declare that there are no conflicts of interest regarding the publication of this paper.

Acknowledgments

The present work has been supported by Ministry of Education and Science, Russian Federation (Project no. 16.7864.2017). The TEM measurements were performed using the shared research facilities of Research and Educational Center for Physics of Solid State Nanostructures at Lobachevsky State University of Nizhny Novgorod.

References

[1] J. Yang and H. Liu, *Metal-Based Composite Nanomaterials*, Springer International Publishing, Switzerland, 2015.

[2] W. Guan, S. Long, R. Jia, and M. Liu, "Nonvolatile resistive switching memory utilizing gold nanocrystals embedded in zirconium oxide," *Applied Physics Letters*, vol. 91, no. 6, Article ID 062111, 2007.

[3] S. V. Tikhov, O. N. Gorshkov, I. N. Antonov, A. P. Kasatkin, and M. N. Koryazhkina, "The forming process in resistive-memory elements based on metal-insulator-semiconductor structures," *Technical Physics Letters*, vol. 40, no. 10, pp. 837–840, 2014.

[4] W.-Y. Chang, K.-J. Cheng, J.-M. Tsai et al., "Improvement of resistive switching characteristics in TiO_2 thin films with embedded Pt nanocrystals," *Applied Physics Letters*, vol. 95, no. 4, Article ID 042104, 2009.

[5] M. H. Lee and C. S. Hwang, "Resistive switching memory: Observations with scanning probe microscopy," *Nanoscale*, vol. 3, no. 2, pp. 490–502, 2011.

[6] M. H. Devoret, D. Esteve, and C. Urbina, "Single-electron transfer in metallic nanostructures," *Nature*, vol. 360, no. 6404, pp. 547–553, 1992.

[7] A. L. Stepanov and I. B. Khaibullin, "Fabrication of metal nanoparticles in sapphire by low-energy ion implantation," *Reviews on Advanced Materials Science*, vol. 9, no. 2, pp. 109–129, 2005.

[8] M. Pelton and G. W. Bryant, *Introduction to Metal-Nanoparticle Plasmonics*, Wiley & Sons, New York, NY, USA, 2013.

[9] P. Banerjee, D. Conklin, S. Nanayakkara, T.-H. Park, M. J. Therien, and D. A. Bonnell, "Plasmon-induced electrical conduction in molecular devices," *ACS Nano*, vol. 4, no. 2, pp. 1019–1025, 2010.

[10] A. Meldrum, R. Lopez, R. H. Magruder, L. A. Boatner, and C. W. White, "Structure and properties of nanoparticles formed by ion implantation," *Topics in Applied Physics*, vol. 116, pp. 255–285, 2010.

[11] S. H. Cho, S. Lee, D. Y. Ku et al., "Growth behavior and optical properties of metal-nanoparticle dispersed dielectric thin films formed by alternating sputtering," *Thin Solid Films*, vol. 447-448, pp. 68–73, 2004.

[12] J. D. McBrayer, R. M. Swanson, and T. W. Sigmon, "Diffusion of Metals in Silicon Dioxide," *Journal of the Electrochemical Society*, vol. 133, no. 6, pp. 1242–1246, 1986.

[13] U. S. Kuzminov, E. E. Lomonova, and V. V. Osiko, *Refractory Materials from the Cold Crucible*, Science, Moscow, Russia, 2004.

[14] S. V. Tikhov, O. N. Gorshkov, D. A. Pavlov et al., "Capacitors with nonlinear characteristics based on stabilized zirconia with built-in gold nanoparticles," *Technical Physics Letters*, vol. 40, no. 5, pp. 369–371, 2014.

[15] O. N. Gorshkov, I. N. Antonov, D. O. Filatov et al., "Forming dense arrays of gold nanoparticles in thin films of yttria stabilized zirconia by magnetron sputtering," *Technical Physics Letters*, vol. 42, no. 1, pp. 36–39, 2016.

[16] O. N. Gorshkov, D. A. Pavlov, V. N. Trushin et al., "Peculiarities in the formation of gold nanoparticles by ion implantation in stabilized zirconia," *Technical Physics Letters*, vol. 38, no. 2, pp. 185–187, 2012.

[17] G. Mie, "Beiträge zur Optik trüber Medien, speziell kolloidaler Metallösungen," *Annalen der Physik*, vol. 330, no. 3, pp. 377–445, 1908.

[18] V. I. Aleksandrov, V. V. Osikov, A. M. Prokhorov, and V. M. Tatarintsev, "The formation of high-temperature materials by direct high-frequency fusion in a cold container," *Russian Chemical Reviews*, vol. 47, no. 3, pp. 213–237, 1978.

[19] B. Auguié and W. L. Barnes, "Collective resonances in gold nanoparticle arrays," *Physical Review Letters*, vol. 101, no. 14, Article ID 143902, 2008.

[20] S. Arnon and E. Rosenkrantz, "Enhanced absorption of light by charged nanoparticles," *Optics Letters*, vol. 35, no. 8, pp. 1178–1180, 2010.

[21] S. V. Tikhov, O. N. Gorshkov, M. N. Koryazhkina, I. N. Antonov, and A. P. Kasatkin, "Specific features of nonequilibrium depletion accompanied by the trapping of minority carriers by surface states in metal–insulator–semiconductor structures," *Technical Physics Letters*, vol. 42, no. 2, pp. 138–142, 2016.

[22] T. Bian, R. Chang, and P. T. Leung, "Optical interactions with a charged metallic nanoshell," *Journal of the Optical Society of America B: Optical Physics*, vol. 33, no. 1, pp. 17–26, 2016.